National Park Service
U.S. Department of the Interior

Natural Resource Stewardship and Science

Mapping Snow Persistence for the Range of the Western Arctic Caribou Herd, Northwest Alaska, Using the Landsat Archive (1985-2011)

Natural Resource Technical Report NPS/ARCN/NRTR—2012/643

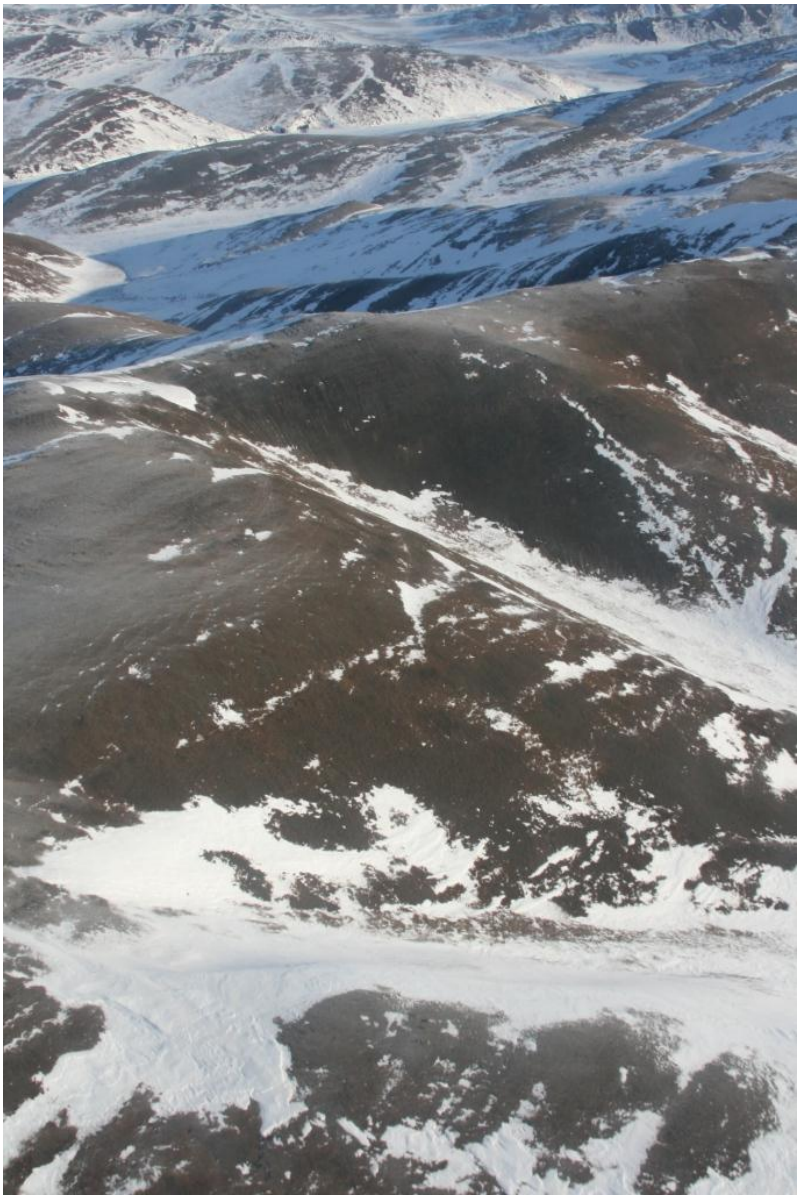

ON THE COVER
Differential snow melt in the Nulato Hills, April 2012.
Photograph by: Kyle Joly

Mapping Snow Persistence for the Range of the Western Arctic Caribou Herd, Northwest Alaska, Using the Landsat Archive (1985-2011)

Natural Resource Technical Report NPS/ARCN/NRTR—2012/643

Matthew J. Macander, Christopher S. Swingley

ABR, Inc.—Environmental Research & Services
P.O. Box 80410
Fairbanks, Alaska 99708-0410

December 2012

U.S. Department of the Interior
National Park Service
Natural Resource Stewardship and Science
Fort Collins, Colorado

The National Park Service, Natural Resource Stewardship and Science office in Fort Collins, Colorado, publishes a range of reports that address natural resource topics. These reports are of interest and applicability to a broad audience in the National Park Service and others in natural resource management, including scientists, conservation and environmental constituencies, and the public.

The Natural Resource Technical Report Series is used to disseminate results of scientific studies in the physical, biological, and social sciences for both the advancement of science and the achievement of the National Park Service mission. The series provides contributors with a forum for displaying comprehensive data that are often deleted from journals because of page limitations.

All manuscripts in the series receive the appropriate level of peer review to ensure that the information is scientifically credible, technically accurate, appropriately written for the intended audience, and designed and published in a professional manner.

Data in this report were collected and analyzed using methods based on established, peer-reviewed protocols and were analyzed and interpreted within the guidelines of the protocols.

Views, statements, findings, conclusions, recommendations, and data in this report do not necessarily reflect views and policies of the National Park Service, U.S. Department of the Interior. Mention of trade names or commercial products does not constitute endorsement or recommendation for use by the U.S. Government.

This report is available from the Natural Resource Publications Management website (http://www.nature.nps.gov/publications/nrpm/).

Please cite this publication as:

Macander, M. J. and C. S. Swingley. 2012. Mapping snow persistence for the range of the Western Arctic Caribou Herd, northwest Alaska, using the Landsat archive (1985-2011). Natural Resource Technical Report NPS/ARCN/NRTR—2012/643. National Park Service, Fort Collins, Colorado.

NPS 953/117759, December 2012

Contents

Contents (continued)

Figures

Page

Tables

Page

Acknowledgments

We thank Kyle Joly and Sarah Stehn with the National Park Service for support and management of this project. Kyle Joly, Dave Swanson and Jim Lawler with the National Park Service provided review of the products. Alex Prichard provided helpful review comments. We give Allison Zusi-Cobb and Alice Stickney a special thanks for producing this report.

Introduction

A critical part of the National Park Service's Arctic Network Inventory and Monitoring Program is monitoring the Western Arctic Caribou Herd (WACH). The status, distribution, movements and trends in the condition of caribou in all five park units are monitored. Accurate and detailed models of snow cover within the range of the Western Arctic Caribou Herd will provide important context to help understand movement patterns and timing of caribou migrations. Snow depth influences caribou winter distribution and habitat availability by impacting the costs of locomotion and cratering for forage plants and lichens. Snow depth patterns on the landscape also influence plant communities, affecting the distribution of preferred forage species.

Physical modeling techniques (e.g. Liston and Hiemstra 2011) and remote sensing methods (e.g. Hall et al. 2001, Brodzik et al. 2007) have been used to provide information on snow cover and snow depth data at daily to weekly timescales, and at spatial resolutions of 500–25,000 m. However, much of the variability in snow cover happens at much finer spatial scales, particularly for mountain and tundra snowpacks (Sturm 1995).

To help characterize winter and spring habitat conditions related to snow depth for the Western Arctic Caribou Herd, we used a combination of image interpretation and statistical modeling to describe patterns of snow persistence on the landscape at fine spatial resolution (30-m pixels). To accomplish this we compiled and analyzed an extensive time series of over 10,000 Landsat images (1985–2011) that covered the caribou range. We used the results of this analysis to map the typical date of snowmelt across the range, which can provide information on the spatial distribution of snow cover patterns relevant to caribou winter habitat quality. Areas wind-scoured during winter generally lack suitable lichen forage, and can be identified because they are often snow-free during winter and early spring. Sites with shallow snow provide easier travel and foraging and they will tend to melt earlier. Deeper snow, which melts later, can make foraging more difficult for caribou.

Snow persistence and snow depth patterns affect other wildlife species, plant communities, hydrologic and aquatic systems, and soil temperatures. For example, polar bears and wolverines locate dens in snow drifts. Snowbed plant communities often include unique species assemblages and have delayed phenology. Late melting snow drifts can help support stream flow during dry summers. Deep snow insulates plants and the soil and can facilitate shrub expansion (Sturm 2001). Many wildlife species use the snow-free lands that are exposed earlier in the season for grazing and nesting.

Methods

Study Area

The study area is based on the WACH range map (Figure 1). The range includes winter range, calving grounds, summer range, migratory areas, and outer range (areas on the periphery of the herd's range that get occasional use) with a total area of 377,519 square kilometers. It covers the northwest portion of Alaska, including portions of the North Slope, Brooks Range, Yukon Basin, Seward Peninsula and Yukon Kuskokwim Delta.

ABR, Inc. developed a statewide tiling scheme in the Alaska Albers (NAD 1983) coordinate system (Figure 2) to facilitate the creation of time-series stacks from overlapping Landsat paths. The study area was expanded to include all full tiles that intersected a portion of the WACH range map. In addition, some extra tiles at the border of the range were included to accommodate possible range expansion and to include the full extent of some conservation units. The final study area included 562 tiles, for a total area of 505,800 square kilometers.

Landsat Image Acquisition

Browse Review

A total of 89 WRS2 path/rows (footprints of individual satellite scenes) covered a portion of the study area (Figure 3). Four of these were excluded because they were mostly ocean and contained no land that was not also included in the adjacent row.

All Landsat 4 TM, Landsat 5 TM, and Landsat 7 ETM+ browse images acquired through late summer 2011 for the remaining 85 WRS2 path/rows were downloaded from the USGS, along with the associated metadata text records. The browse images were georeferenced by creating a GIS-readable world file from the information in the metadata file using a custom Python script. The browse images were organized into folders by WRS2 path and row. To facilitate sorting for review, they were renamed by prepending the date (in MM_DD_YYYY) format to each browse image filename.

Each Landsat path/row was reviewed manually and browse images which contained useful information about ground conditions (even over only a portion of the scene) were identified. Any GIS viewer or generic photo viewer could be used for this purpose as long as there is a way to flag the useful scenes to generate a computer-readable list.

Image Downloads

Lists of Landsat granules were compiled and were submitted to the USGS Landsat bulk download page (http://earthexplorer.usgs.gov/order/bulkdownload). Initially, a full list was submitted to determine which scenes were already available online. Scenes that were not already available for download were re-packaged into order lists (maximum 100 TM, 100 ETM+ SLC-On, and 100 SLC-Off scenes per order list). The order lists were resubmitted to the Landsat Bulk Download page and the imagery was ordered.

When the imagery was ready for download, a script was used to download each scene in tar.gz format. The scene was unpacked and was organized into raw data folders in a hierarchy of path, row, and scene. The individual TIF bands were gzipped for storage in the raw data directories to

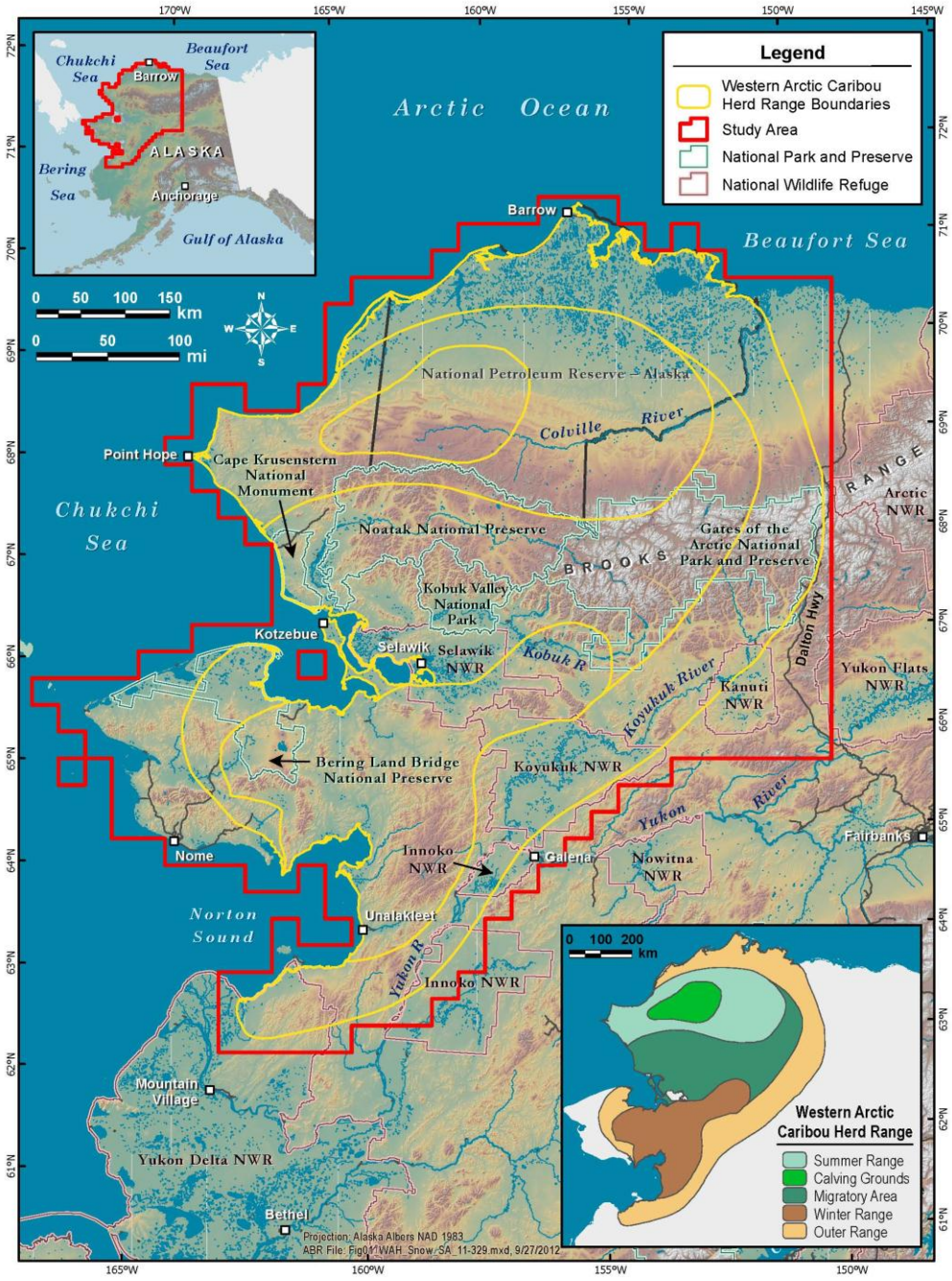

Figure 1. Study area overview, Western Arctic Caribou Herd Range, Alaska.

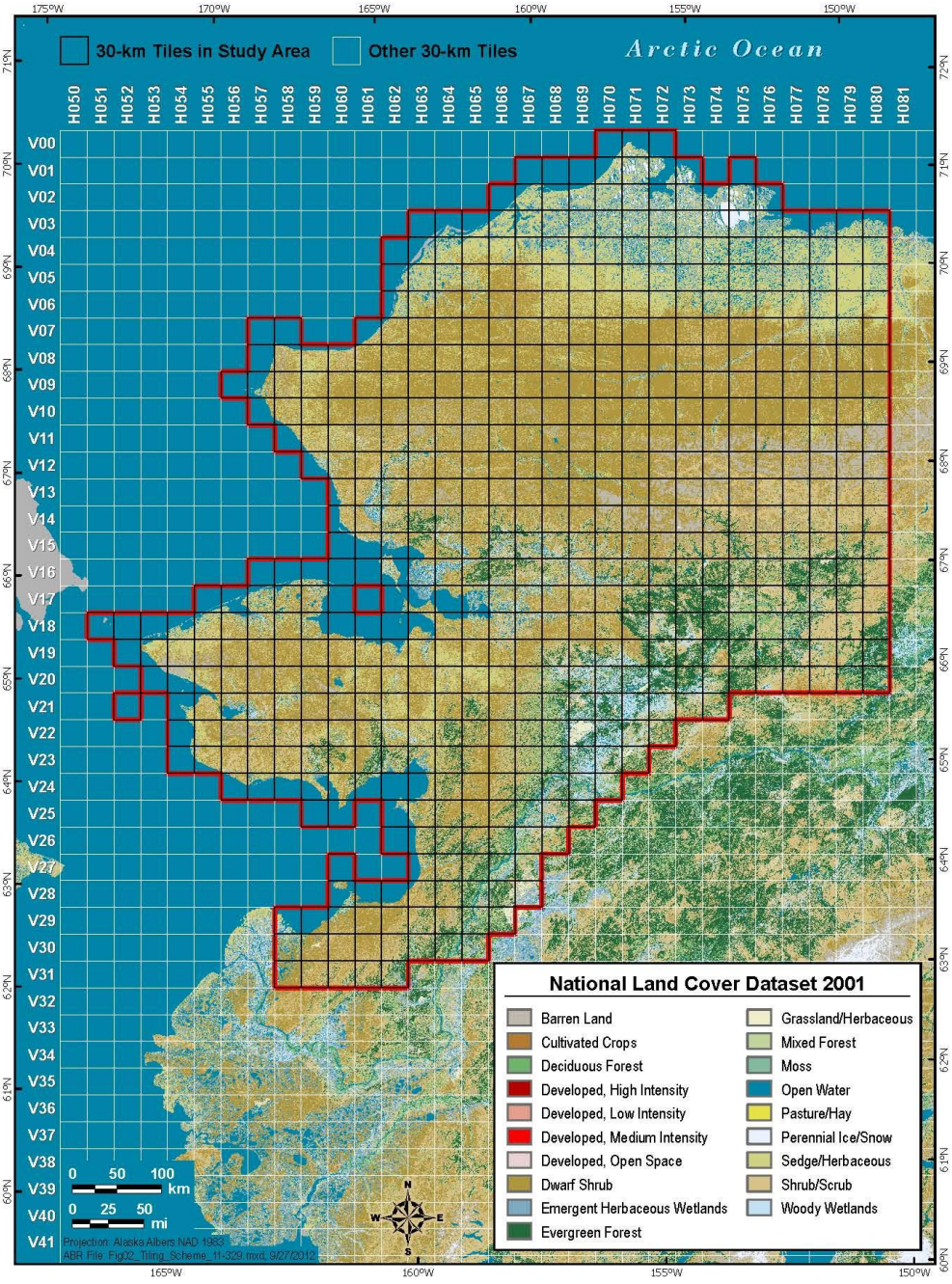

Figure 2. Tiling scheme for Landsat data in the study area.

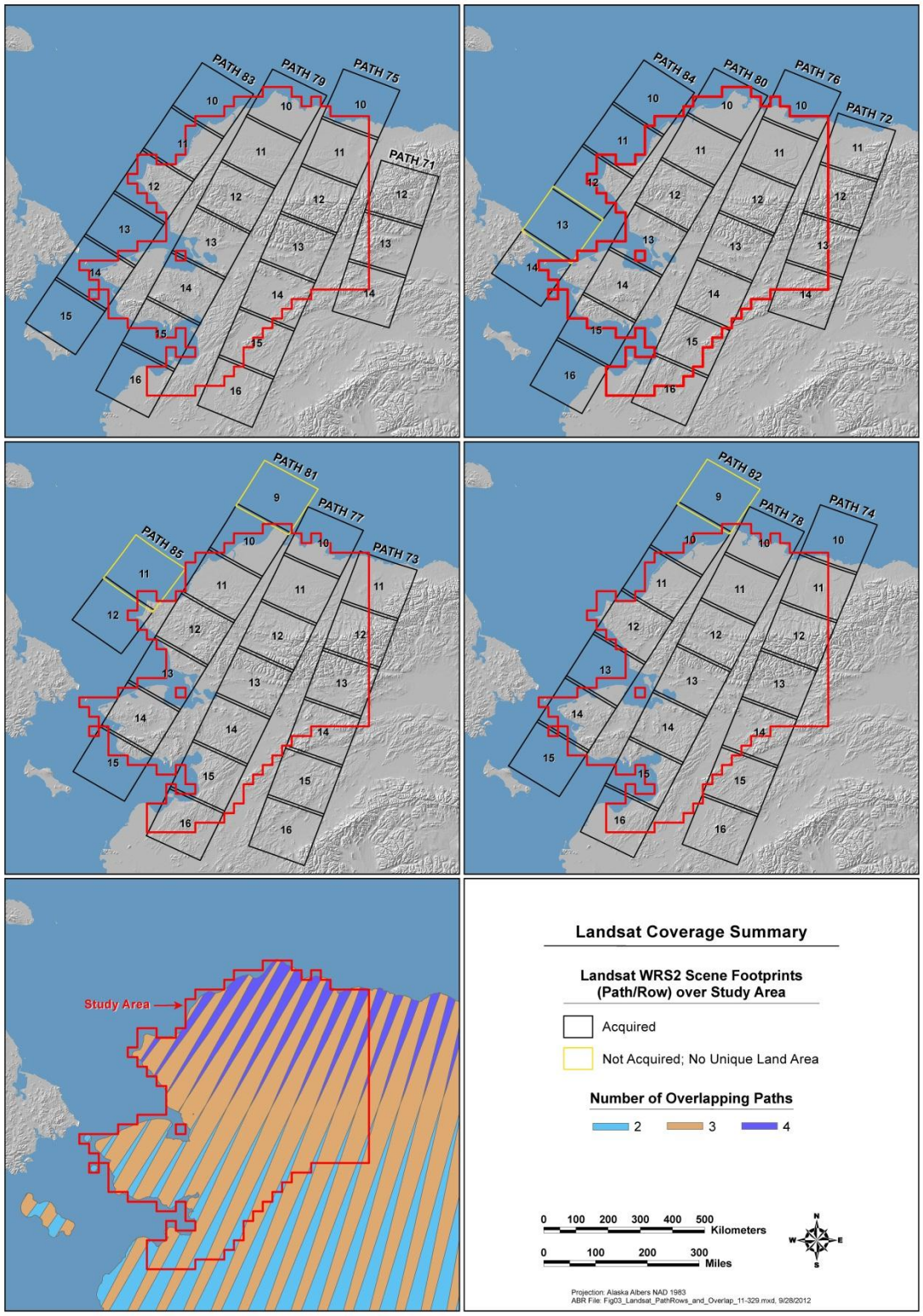

Figure 3. Landsat WRS2 path/row coverage over the study area.

allow for more efficient access to individual files while minimizing the storage requirements of the raw data.

Landsat Image Preprocessing

Preprocessing steps included extraction of relevant metadata, calibration to top-of-atmosphere reflectance, and calculation of a cloud mask for each scene. These steps were performed using the Landsat Ecosystem Disturbance Adaptive Processing System (LEDAPS, Masek 2006).

Metadata

The LEDAPS *lndpm* script ingests both NLAPS and LGPS format Landsat data and produces a text file with consistent metadata fields including acquisition date and time, processing date and time, calibration parameters such as bias and gain, projection, and the solar geometry for the scene center (solar zenith and solar azimuth). The *lndpm* script also generates the parameter files necessary for the other LEDAPS scripts. Two metadata fields that were not provided by *lndpm* (***processing_software_version*** and ***processing_level***) were extracted for each scene by a custom Python script. The key metadata fields are defined in Table 1. The metadata for each scene was imported into a PostgreSQL database.

The metadata tables were reviewed to identify the processing level for each scene. Terrain Corrected (L1T) scenes have very precise geolocation based on the inclusion of ground control points from Landsat GeoCover images. These scenes are accurately coregistered to each other (generally within one 30-m pixel). Systematic Corrected (L1G) scenes lack ground control points and have lower geolocation precision. Only L1T scenes were used for the analysis.

Calibration To Top-Of-Atmosphere Reflectance

We standardized each scene to top of atmosphere reflectance using the LEDAPS *lndcal* algorithm, which calculates top-of-atmosphere reflectance using the scene metadata and calibration coefficients from the Landsat 7 Science Data Users Handbook (http://landsathandbook.gsfc.nasa.gov/handbook.html). Landsat 4 and 5 data were calibrated using the coefficients from Chander et al. (2009).

Cloud Mask

The LEDAPS *lndcsm* algorithm was used to calculate a cloud mask using the Automated Cloud-Cover Assessment algorithm (ACCA, Irish 2006). The cloud mask identified each pixel as gap, cloud, or cloud-free based on the ACCA algorithm. Gap values occurred either beyond the edge of the image, or in wedge-shaped gaps caused by the scan-line corrector malfunction on Landsat 7 images acquired after May 2003. Cloud shadows were not detected by *lndcsm*.

Shadow Modeling

The study contains extensive areas of hilly and mountainous terrain, where dark, shadowed terrain is extensive in satellite images. Sun angles are low at high latitudes, particularly in early- to mid-winter and late summer, increasing the extent of shadowing. Modeling, described below, was used to identify the areas in each Landsat scene that were potentially affected by terrain shadowing. Within these areas, a modified snow mapping algorithm was applied.

Digital Elevation Model (DEM)

DEM data are required inputs for calculation of solar incidence angle and terrain shadowing. Two sources of DEM data were considered: the National Elevation Dataset (NED) and the

Table 1. Key metadata fields for each Landsat scene.

Metadata Field Name	Field Type	Description
sceneid	Text	Landsat Granule ID; unique identifier in USGS archive.
full_sceneid	Text	Landsat Granule ID concatenated with Production Date; unique identifier for reprocessed scenes .
base_sceneid	Text	Landsat Granule ID excluding the version number; uniquely identifies a collected scene.
production_date	Date	Date when the raw L0R data was processed to L1T or L1G format.
satellite	Text	Satellite platform.
instrument	Text	Satellite instrument.
acquisition_date	Date	Date when the raw L0R data was processed to L1T or L1G format.
solar_zenith	Float	Solar zenith angle (degrees) for scene center.
solar_azimuth	Float	Solar azimuth angle (degrees) for scene center.
wrs_system	Integer	World Reference System (WRS) used as basis for scene paths and rows.
wrs_row	Integer	Row of scene in the World Reference System.
wrs_path	Integer	Path of scene in the World Reference System.
nband	Integer	Number of reflective bands.
pixel_size	Float	Pixel size of reflective bands, m.
projection_zone	Integer	UTM projection zone.
ulx	Float	Corner coordinate easting for the upper left pixel.
uly	Float	Corner coordinate northing for the upper left pixel.
gain	Text vector	Radiometric calibration gain values per reflective band.
bias	Text vector	Radiometric calibration bias values per reflective band.
product_type	Text	Level of processing completed for the scene.
processing_system	Text	Name and version of processing software used to process the scene from raw L0R data.

Advanced Spaceborne Thermal Emission and Reflection Radiometer (ASTER) Global Digital Elevation Model Version 2 (G-DEM2), a product of Japan's Ministry of Economy, Trade and Industy (METI) and the National Aeronautical and Space Administration (NASA). The ASTER G-DEM has higher resolution and is based on data that is much more recent than the NED.

The G-DEM2 was selected for the terrain shadow modeling because it appeared to do a better job of representing shadows in areas of mountainous terrain. The GDEM-2 was more detailed and accurate than the NED in areas of high relief. Artifacts were abundant, including many artificial bumps and valleys. The effect of such artifacts was to create some modeled shadows that did not actually occur. Such artifacts probably covered <1% of the area, though the shadows cast by artifacts may have approached or exceeded 1% of the area when sun elevation was low. However, the only consequence of the G-DEM2 artifacts for the current study was to cause a modified snow mapping algorithm to be applied.

The G-DEM2 data were mosaicked and were then reprojected to 30-m resolution using a cubic convolution kernel into UTM zones that covered the extent of the Landsat imagery. The cubic convolution kernel was used because it better preserves the peaks and valleys of the input data; the peaks in particular were important factors controlling terrain shadows. Terrain slope (degrees) and aspect (degrees) were calculated from the reprojected G-DEM2 data.

Solar Incidence Angle

Solar incidence angle is the angle between the incoming solar radiation and a line normal to the terrain. The solar incidence angle is zero for slopes directly facing the sun, e.g. a flat surface when the sun is directly overhead. Surfaces with a solar incidence angle greater than 90 degrees are facing away from the sun, and are shadowed. Surfaces with very low positive solar incidence angles are also likely to be shadowed, because vegetation and other rough surface features can cast shadows.

The solar incidence angle was calculated for each pixel in each scene using the G-DEM2 slope and aspect rasters, combined with the scene center solar geometry values from the scene metadata:

$$i = \arccos [\cos \theta \cos e + \sin \theta \sin e \cos(\varphi_m - \varphi_s)]$$

where θ = solar zenith angle, φ_s = solar azimuth, e = terrain slope, and φ_m = terrain aspect.

The results of the solar incidence angle were reviewed interactively and a threshold identifying pixels that were generally dark was identified. These pixels were considered potential shadows for the snow mapping.

Terrain Shadows

Surfaces with a with a solar incidence angle greater than 90 degrees are facing away from the sun, and are shadowed; however, additional shadows occur on surfaces that are facing the sun but have intervening terrain blocking the sun. The ArcGIS Hillshade tool includes an option to model these shadows. The Hillshade tool was run for each scene using the G-DEMV2 and solar geometry from the metadata as inputs. The Hillshade tool identified shadowed terrain with a "zero" coded in the hillshade.

Shadow Model

A shadow model was calculated for each scene by combining the shadows identified by the solar incidence angle and by the terrain shadow (Hillshade) rasters. If the Hillshade value was zero, the shadow raster was set to a value outside the range of the solar incidence angles (200); otherwise, the value of the shadow raster was set to equal the solar incidence angle raster. In this way, a shadow threshold could be set identified when an appropriate solar incidence angle threshold value was determined. The hillshade-derived terrain shadows would always be included as shadow because of their high value in the shadow model raster.

Snow Mapping

Snowmap

The Snowmap algorithm (Hall et al. 1995, 2001) was used to generate a binary map of the presence or absence of snow for all non-fill (i.e. not image gap), non-shadow pixels. Snow is one

of the only natural materials that is both highly reflective in visible wavelengths and absorbed in the middle infrared wavelengths; therefore, satellite snow-mapping algorithms are based on these properties. The Normalized Difference Snow Index (NDSI) tends to be high when snow is present in a remote sensing pixel and is calculated from the visible and short-wavelength infrared wavelengths as follows:

$$NDSI = (VIS - SWIR) \div (VIS + SWIR)$$

Where:

VIS = Top-of-atmosphere reflectance in a visible wavelength, typically about 0.55 micrometer (μm). Landsat TM and ETM+ band 2.

SWIR = Top-of-atmosphere reflectance in a short-wavelength infrared, typically about 1.64 μm. Landsat TM and ETM+ band 5.

The Snowmap algorithm (Hall et al., 2001) classifies pixels as snow if the following conditions are met: NDSI is greater than 0.4, visible reflectance (Landsat TM and ETM+ band 3) is greater than 0.10, and near-infrared reflectance (NIR, about 0.85 μm; Landsat TM and ETM+ band 4) reflectance is greater than 0.11.

Shadow Snowmap

The standard Snowmap algorithm frequently misclassified shadowed pixels as snow-free. The visible reflectance and near-infrared tests are intended to prevent dark materials such as water from being mistakenly mapped as snow. However, all surfaces in deep shadows may be dark, and hence one or both of the reflectance tests fail and the shadowed pixel is classified as snow-free.

To prevent shadows from being misclassified as snow-free, the two reflectance tests were dropped for pixels where modeled shadows were present. Only the NDSI test was applied. The shadow Snowmap algorithm classifies pixels as snow if the following condition is met: NDSI is greater than 0.4.

Cloud/Shadow/Snow Map

The *lndcsm* algorithm identified each pixel as cloud, cloud-free, or gap (missing data). The shadow model classified each pixel as shadow or sunny. Finally, the Snowmap and Shadow Snowmap algorithms identified each pixel as snow or snow-free. The results from these four models were combined to describe the cloud, shadow and snow status of each pixel in each scene (Table 2). The detailed outputs were used to assess the performance of the cloud and snow algorithms visually. For the time series analysis, only the cloud-free pixels were utilized, and only the snow status (snow or snow-free) was extracted.

Time Series Analysis

Landsat 30 Km Tile Preparation

The results of the cloud/shadow/snow mapping model were compiled for each of the 562 30x30 km tiles in the study area. The tiles combine data from different Landsat paths and rows and different source projections into a format with standardized projection and dimensions. The tile

Table 2. Lookup table for combining cloud/shadow/snow map algorithms.

Cloud-mask Algorithm (*lndcsm*)	Shadow Model	Snowmap	Shadow Snowmap	cloud	shadow	snow	css Value	Detailed Result	Snow-Free Date Algorithm Input
Cloud	Shadow	Snow	Snow	1	1	1	111	Cloudy	No Data
Cloud	Shadow	Snow	Snow-free	1	1	0	110	Cloudy	No Data
Cloud	Shadow	Snow-free	Snow	1	1	1	111	Cloudy	No Data
Cloud	Shadow	Snow-free	Snow-free	1	1	0	110	Cloudy	No Data
Cloud	Sunny	Snow	Snow	1	0	1	101	Cloudy	No Data
Cloud	Sunny	Snow	Snow-free	1	0	1	101	Cloudy	No Data
Cloud	Sunny	Snow-free	Snow	1	0	0	100	Cloudy	No Data
Cloud	Sunny	Snow-free	Snow-free	1	0	0	100	Cloudy	No Data
Gap	Shadow	Snow	Snow	255	1	1	255	Gap	No Data
Gap	Shadow	Snow	Snow-free	255	1	0	255	Gap	No Data
Gap	Shadow	Snow-free	Snow	255	1	1	255	Gap	No Data
Gap	Shadow	Snow-free	Snow-free	255	1	0	255	Gap	No Data
Gap	Sunny	Snow	Snow	255	0	1	255	Gap	No Data
Gap	Sunny	Snow	Snow-free	255	0	1	255	Gap	No Data
Gap	Sunny	Snow-free	Snow	255	0	0	255	Gap	No Data
Gap	Sunny	Snow-free	Snow-free	255	0	0	255	Gap	No Data
Cloud-free	Shadow	Snow	Snow	0	1	1	011	Snow based on Shadow Snowmap	1 (Snow Present)
Cloud-free	Shadow	Snow	Snow-free	0	1	0	010	Snow-free based on Shadow Snowmap	0 (Snow Absent)
Cloud-free	Shadow	Snow-free	Snow	0	1	1	011	Snow based on Shadow Snowmap	1 (Snow Present)
Cloud-free	Shadow	Snow-free	Snow-free	0	1	0	010	Snow-free based on Shadow Snowmap	0 (Snow Absent)
Cloud-free	Sunny	Snow	Snow	0	0	1	001	Snow based on Snowmap	1 (Snow Present)
Cloud-free	Sunny	Snow	Snow-free	0	0	1	001	Snow based on Snowmap	1 (Snow Present)
Cloud-free	Sunny	Snow-free	Snow	0	0	0	000	Snow-free based on Snowmap	0 (Snow Absent)
Cloud-free	Sunny	Snow-free	Snow-free	0	0	0	000	Snow-free based on Snowmap	0 (Snow Absent)

size results in an array of 1000x1000 30-m pixels, which allows hundreds of layers in the time series to be stored in memory for analysis.

The compilation for each tile was performed by a Geospatial Data Abstraction Library (GDAL) script. The script reprojected the cloud/shadow/snow map from the default UTM projection to Alaska Albers (NAD 1983); clipped the imagery to the extent of each tile; and, if necessary, mosaicked adjacent Landsat rows from the same acquisition date together. The nearest neighbor resampling method was used during reprojection and the 30-m pixel size was maintained. The tiling approach is very similar to that used by the Web Enabled Landsat Data project (WELD, Roy et al. 2010), but was different in particulars including the depth of the Landsat record available and the size, naming and alignment of tiles. At the time of our analysis the WELD data record only include a portion of the Landsat 7 ETM+ data record while our analysis includes all Landsat 4, 5 and 7 TM and ETM+ scenes. The tiles used for our analysis are smaller than the WELD tiles (1000x1000 pixels instead of 5000x5000 pixels) because of the very large number of timesteps (hundreds) that need to be loaded into memory for each tile. Finally, the WELD data at the time of our analysis did not align with other statewide 30-m datasets such as the NLCD2001 land cover layer, while our tiles are aligned and coregistered with these ancillary datasets.

A Python script was run to summarize the pixel counts for each tile and scene. The results were stored in the PostgreSQL database. The number of valid pixels (sunny snow, shadowed snow, sunny snow-free, and shadowed snow-free) was calculated for each tile and scene.

Landsat Time Series Preparation

The set of cloud/shadow/snow maps for each tile was filtered to select all scenes with valid data and acquisition dates between February 1 and August 31. Due to cloud cover and slight shifts in the location of Landsat paths, some tiles contained no data from a particular scene and these were excluded from further analysis. Dates after August 31 were more likely to have recent autumn snow, complicating the detection of the snow melt date. The resulting set of cloud/shadow/snow maps (*css*) for each tile was stacked into a virtual dataset (VRT) using GDAL. The Julian date (day of year, *doy*) for each layer in the stack was tracked. For analysis, both gaps and clouds were treated as unknown and shadow status was ignored; the relevant response variable was the binary snow presence (1) or absence (0).

Snow Persistence Algorithm

To identify the day of year value that best separated the snow-covered from the snow-free season, we analyzed the *css* stack and *doy* vector in R using a binary classification tree (rpart), which was constrained to one split. Logistic regression is an alternate statistical technique that could be used; however, the classification tree was selected because it is less influenced by outliers. For each pixel, the split value (Julian date) that provided the best split between the snow-covered (1) and snow-free (0) season was extracted. The direction of the split (left or right) was extracted; a right split corresponded to the unusual circumstance when the best split was from a snow-free condition to a snow-covered condition. The split value was stored in the sf_doy_f raster layer, as a floating point number (the name stands for Snow-Free Day Of Year Float); right splits were stored as negative values. Other values extracted included n (the count of cloud-free observations), n_snow (the count of cloud-free observations with snow), n_snowfree (the count of cloud-free observations with no snow), n_snow_correct (the count of cloud-free

observations with snow that are correctly classified by the split value in sf_doy_f, assuming the snow state was correctly mapped), and n_snowfree_correct (the count of cloud-free observations that are snow-free that are correctly classified by the split value in sf_doy_f, again assuming the snow state was correctly mapped).

The sf_doy_f output raster is coded with the Julian date that the pixel typically becomes snow-free. For performance and visualization reasons, the raster was converted to an 8-bit unsigned integer sf_doy (for Snow-Free Day of Year), with values 0–255. Because a date filter was used in the analysis (February 1–August 31), valid values returned by the classification tree algorithm were between Julian dates 60–244. Values outside this range were special cases, and were filled using an alternative approach.

The special cases occurred either when there was no split, or when the split was reversed (i.e., from snow-free to snow-covered). To fill the values for the special cases, the proportion of snow (p_snow) was calculated by dividing n by n_snow. The p_snow value was used to fill in the sf_doy values for the no split and reverse split cases as follows: if p_snow ≤ 0.25, the condition was defined as "Usually snow-free" and the value was set to 1. If p_snow ≥ 0.70 the condition was defined as "Usually snow-covered" and the value was set to 254. If $0.25 <$ p_snow < 0.75, the condition was defined as "no pattern" and the value was set to 0. The value 255 was reserved for No Data, i.e., pixels that occur within the extent of the raster but are outside the study area.

Assessment and Validation

The internal consistency of the snow-free date algorithm was assessed by calculating the proportion of correct classifications for each pixel, based on the modeled snow-free date and the input stack of snow/snow-free/nodata observations by day of year. The sum of snow observations before the snow-free date, and snow-free observations on or after the snow-free date was divided by the total number of cloud-free observations.

The snow mapping algorithm will correctly map snow that occurs on ice over water bodies, but it can perform unreliably over snow-free ice, flooded ice, and turbid water bodies. The analysis was performed over the entire study area of 562 tiles, which includes many lakes and rivers and extensive coastal and offshore waters around the edge of the study area. The internal consistency assessment was summarized using the full study area, and was also summarized for only the land portion of the study area. For the land portion, water was masked by excluding the “Open Water” class from the National Land Cover Database circa 2001 (NLCD2001).

Data from SNOwpack TELemetery (SNOTEL) sites operated by the National Resource Conservation Service within the study area were compiled. The snow-free date in spring was calculated for each site and for each available year with data for sites with snow depth and/or snow water equivalent data. For snow depth, the snow-free date was identified as the first date with zero inches snow depth. Similarly, for water equivalent, the first date with zero inches water equivalent was identified as the snow-free date. If both snow depth and water equivalent data were available for a particular winter, the water equivalent data was used to determine the snow-free date. The mean snow-free date for each site was calculated from all years with SNOTEL data during the snowmelt season. The SNOTEL site locations were overlaid on the snow-free date map generated from the Landsat analysis and the results from the SNOTEL data and the

Landsat analysis were compared using the value of the Landsat pixel that intersected the SNOTEL location.

Results

Landsat Image Acquisition

Due to the converging polar orbit of the Landsat satellites, the amount of overlap between adjacent paths increased towards the northern portion of the study area (Figure 3). A total of 11,811 TM and ETM+ scenes of interest were identified for the 85 WRS2 path/rows reviewed and the list was submitted to the USGS for processing. 166 scenes could not be processed, likely do some missing ancillary data. The USGS indicates that it is possible that some of these may be processed in the future. The remaining 11,645 were processed by USGS and downloaded for analysis.

Landsat Image Preprocessing

Of the 11,645 Landsat TM and ETM+ scenes acquired from the USGS, 10,913 were successfully processed to the systematic terrain corrected (L1T) product; only these scenes were used for the snow persistence day analysis. A summary of L1T scenes by month and year (Table 3) demonstrates that while there was some Landsat TM data as early as September 1984, the volume of early season (January–May) imagery was very limited prior to the launch of Landsat 7 in late 1999. The current analysis included data for February 1–August 31, 1985–2011, but was heavily weighted towards the 2000–2011 period. Overall, 91% of the scenes used for the current analysis were from the 2000–2011 time period. Note, however, that none of the TM imagery—which includes all pre-2000 data—was impacted by the scan-line corrector malfunction, so it provides high quality, gap-free coverage when available.

The number of images from each path/row was fairly uniform (Table 4, Figure 4), with well over 100 scenes with useable imagery for each path/row except some path/rows at the edge of the study area, which were often mostly ocean and sea ice. Note that, for visualization purposes, Figure 4 depicts the "Thiessen polygons" for the nominal center point of each WRS2 path/row; these are constructed with no overlap or gaps and are much smaller than the actual footprints. There are more scenes available towards the east of the study area. There were fewer scenes available towards the north; this is likely because darkness is more prolonged further north in midwinter, and scenes are generally not acquired when it is dark.

All of the scenes were processed to top of atmosphere reflectance except for seven scenes with solar elevation below zero (i.e. the sun was below the horizon at the scene center). These scenes were all acquired in November or December. In total 10,906 scenes were calibrated to top of atmosphere reflectance.

The LEDAPS cloud mask algorithm (*lndcsm*) was completed for the same set of 10,906 scenes. The cloud mask appeared to perform well for optically thick clouds (see Figure 5, column 2). The cloud mask algorithm also reliably flagged data gaps at image edges as well as those caused by the Landsat 7 scan-line corrector malfunction (SLC-OFF) that affects all Landsat 7 data acquired after May 2003. Some limitations of the cloud mask algorithm were observed: cloud shadows were not identified; clouds were sometimes not identified when saturation occurred in one or more spectral bands due to the calibration setting of the sensor; thin clouds were not reliably identified; some patchy snow was misinterpreted as cloud; and occasionally spurious clouds were detected along the edges of SLC_OFF gaps. The frequency and effect of these

Table 3. Scene count by month and year for all scenes available for the snow-free date analysis. The highlighted cells identify the date ranges used for the current analysis.

Year	Jan.	Feb.	March	April	May	June	July	Aug.	Sept.	Oct.	Nov.	Dec.	Total
1984									1				1
1985				10	9	22	48	30	32	25	40		216
1986			3		16	69	50	55	35	52	25	2	307
1987							6	4	4		6		20
1988					3	6	9	11					29
1989							7	8		3			18
1990						2	3	6	1				12
1991						8	9	19					36
1992						49	57	32	2				140
1995						1	22	39	58	27			147
1999						14	40	87	81	89	34		345
2000	9	30	78	101	100	121	84	51	63	70	16		723
2001			108	109	108	123	70	70	73	72	39		772
2002	11	66	117	101	119	109	95	89	71	33			811
2003		2	121	98	73		47	69	45	20			475
2004		3	107	116	78	107	71	80	58	21			641
2005		5	70	91	84	157	141	102	91	69			810
2006		8	94	107	121	143	144	127	105	15			864
2007		9	99	74	116	105	131	185	91	30			840
2008		9	71	63	151	163	153	168	123	27			928
2009		1	109	126	175	177	174	145	81	26			1014
2010		3	97	69	121	152	94	125	181	45			887
2011		7	119	124	218	175	113	78	43				877
Total	20	143	1193	1189	1492	1703	1568	1580	1239	624	160	2	10913
% of scenes: 2000-2011	100%	100%	100%	99%	98%	90%	84%	82%	83%	69%	34%	0%	88%

Table 4. List of WRS2 Path/Rows with scene count.

Path	Row	Scene Count	Path	Row	Scene Count
71	12	174	78	12	140
71	13	162	78	13	157
71	14	172	78	14	146
72	11	162	78	15	156
72	12	173	78	16	137
72	13	163	79	10	103
72	14	154	79	11	117
73	11	141	79	12	160
73	12	154	79	13	161
73	13	149	79	14	141
73	14	149	79	15	144
73	15	150	79	16	108
73	16	143	80	10	104
74	10	78	80	11	119
74	11	130	80	12	147
74	12	156	80	13	151
74	13	151	80	14	149
74	14	149	80	15	139
74	15	134	80	16	81
74	16	138	81	10	95
75	10	96	81	11	117
75	11	133	81	12	148
75	12	156	81	13	140
75	13	143	81	14	143
75	14	151	81	15	144
75	15	139	82	10	84
75	16	148	82	11	119
76	10	84	82	12	136
76	11	116	82	13	126
76	12	156	82	14	128
76	13	168	82	15	92
76	14	152	83	10	28
76	15	147	83	11	109
76	16	148	83	12	128
77	10	95	83	13	85
77	11	114	83	14	115
77	12	160	83	15	58
77	13	162	84	10	9
77	14	156	84	11	30
77	15	144	84	12	121
77	16	134	84	14	113
78	10	85	85	12	2
78	11	114			
Subtotal		6083			4830
Total					10913

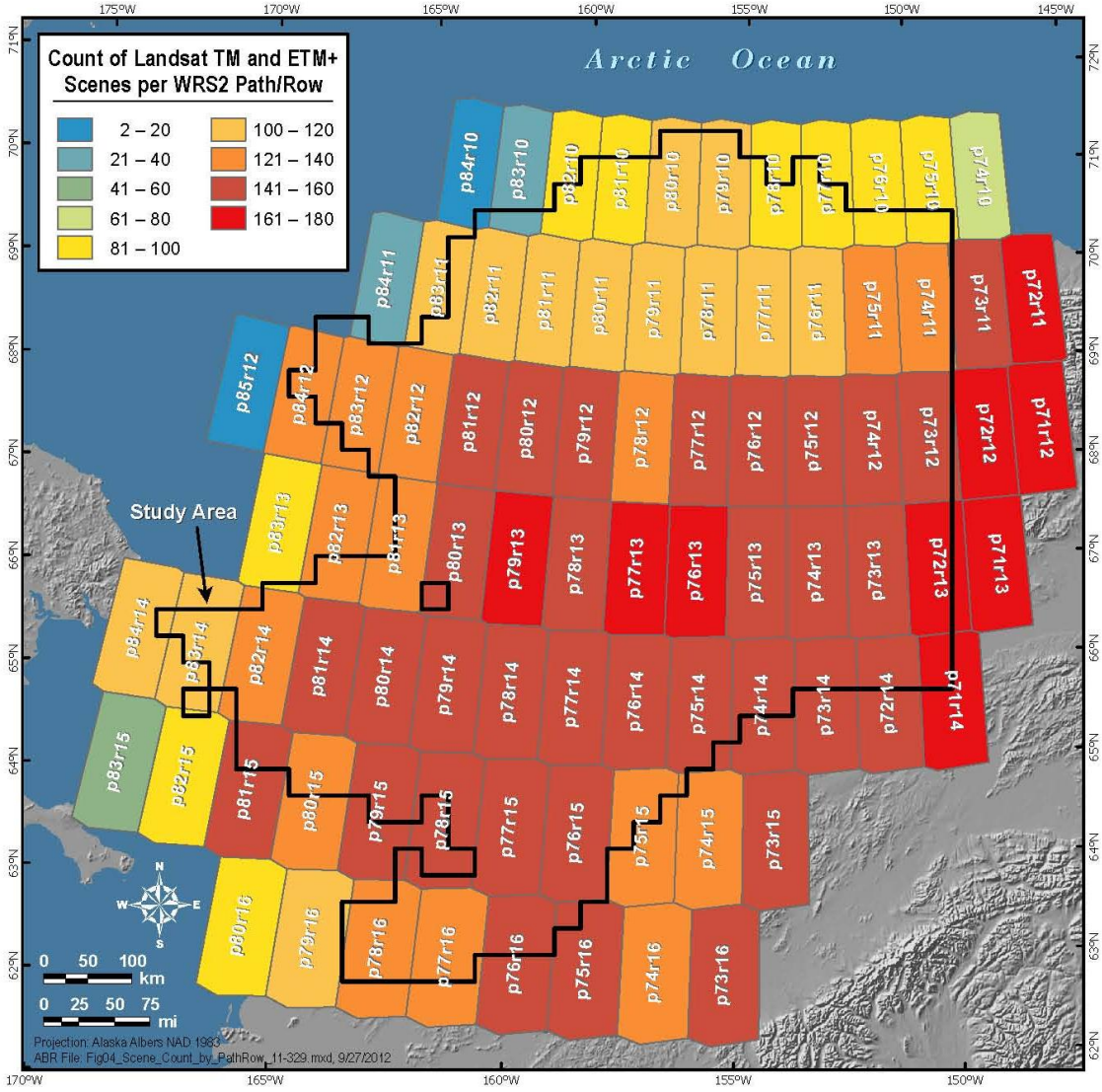

Figure 4. Summary of scene count by path/row.

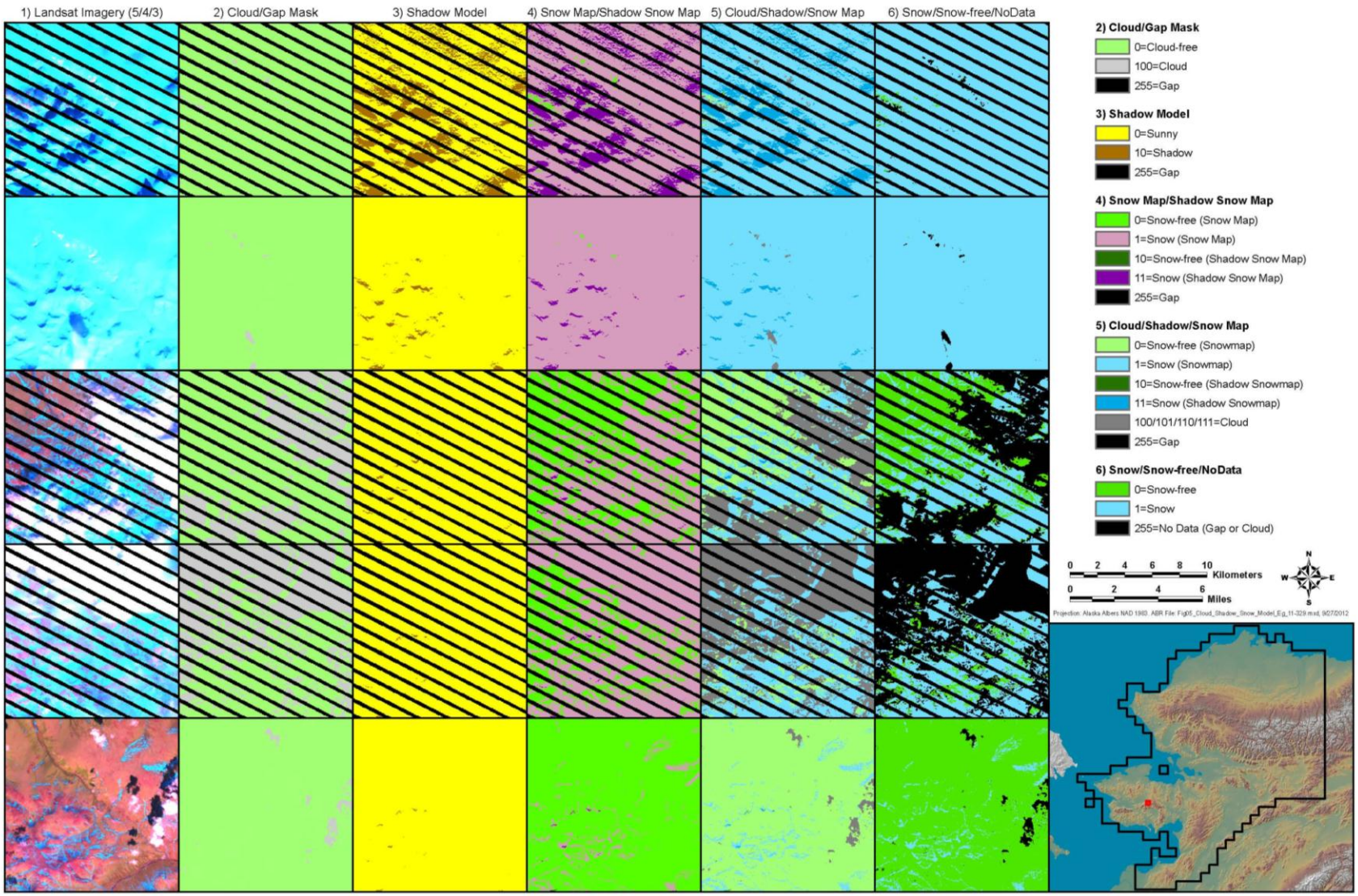

Figure 5. Examples of cloud mask, shadow model, and snow mapping algorithm results.

limitations was not assessed for the current effort. The saturation issue is likely the most important limitation.

Shadow Modeling

Based on visual review of incidence angle outputs and imagery, shadows were identified for surfaces with incidence angles greater than or equal to 80 degrees. The GDEM-2 DEM provided the surface model and the solar zenith and solar azimuth values provided in the metadata for each scene provided the solar geometry parameters. Shadows were much more pronounced in midwinter when solar angles were low (Figure 5, column 3); shadows reach a minimum at the summer solstice and then increase as summer proceeds. The selected threshold of 80 degrees was somewhat liberal for shadow mapping (i.e. it tended to map shadows aggressively, including some areas without visible shadowing, but missing few real shadows). A liberal threshold was used because the shadow snow map algorithm (see next section) should be more resistant to error in non-shadow conditions compared to the standard snow map algorithm in shadow conditions.

Snow Mapping and Cloud/Shadow/Snow Map

Examples of the snow map and shadow snow map outputs (Figure 5, column 4) demonstrate the importance of including a cloud mask. Clouds are often falsely identified as snow; however, when combined with the cloud mask (Figure 5, column 5) the snow state is captured for the non-cloudy land surface. The detailed cloud/snow/shadow map (Figure 5, column 5) is used to derive the simplified snow/snow-free/nodata map (Figure 5, column 6) used for the time series analysis. In midwinter, it captures the landscape pattern of complete or near-complete snow cover, with only scour areas exposed. During spring, the snow-free area increases as lower elevation and shallower snow areas tend to be exposed. Finally, in late spring/early summer only snow drifts remain; some drifts may persist well into late summer or remain as permanent snow fields.

Time Series Analysis

After the preprocessing and tiling had been completed, the computation of snow-free data using the binary classification tree model required about two hours per tile, with each tile comprising one million 30-m pixels. Completing this analysis for the 562 tiles in the study area in a reasonable amount of time required spreading the load across multiple processing cores. This was achieved by using multiple computers but could also be achieved with a single server with sufficient cores and memory.

The binary classification tree returned a snow-free date (the day of year that split the snow season from the snow-free season) for 99.84% of the study area (Figure 6). Broadly, most snowmelt over land occurs from late April through early June, with timing delayed further north and at higher elevations such as in the Brooks Range.

Many local scale snow patterns are evident in the results (Figure 7). Wind redistribution of snow frequently results in snowdrifts at terrain breaks that melt much later than surrounding areas. Examples in relatively flat terrain are seen in tiles a/b/c/f; mountain snow drifts are seen in tiles g/h/k). In rounded terrain without terrain breaks, snow redistribution can result in snow accumulating at valley bottoms, as in tiles a, e, and l.

Windswept, scoured patches that melt out earlier than the surrounding landscape often occur near snow drifts, as in tiles a/e/k/l. Early melt from dust shadow (more rapid snowmelt as a result of

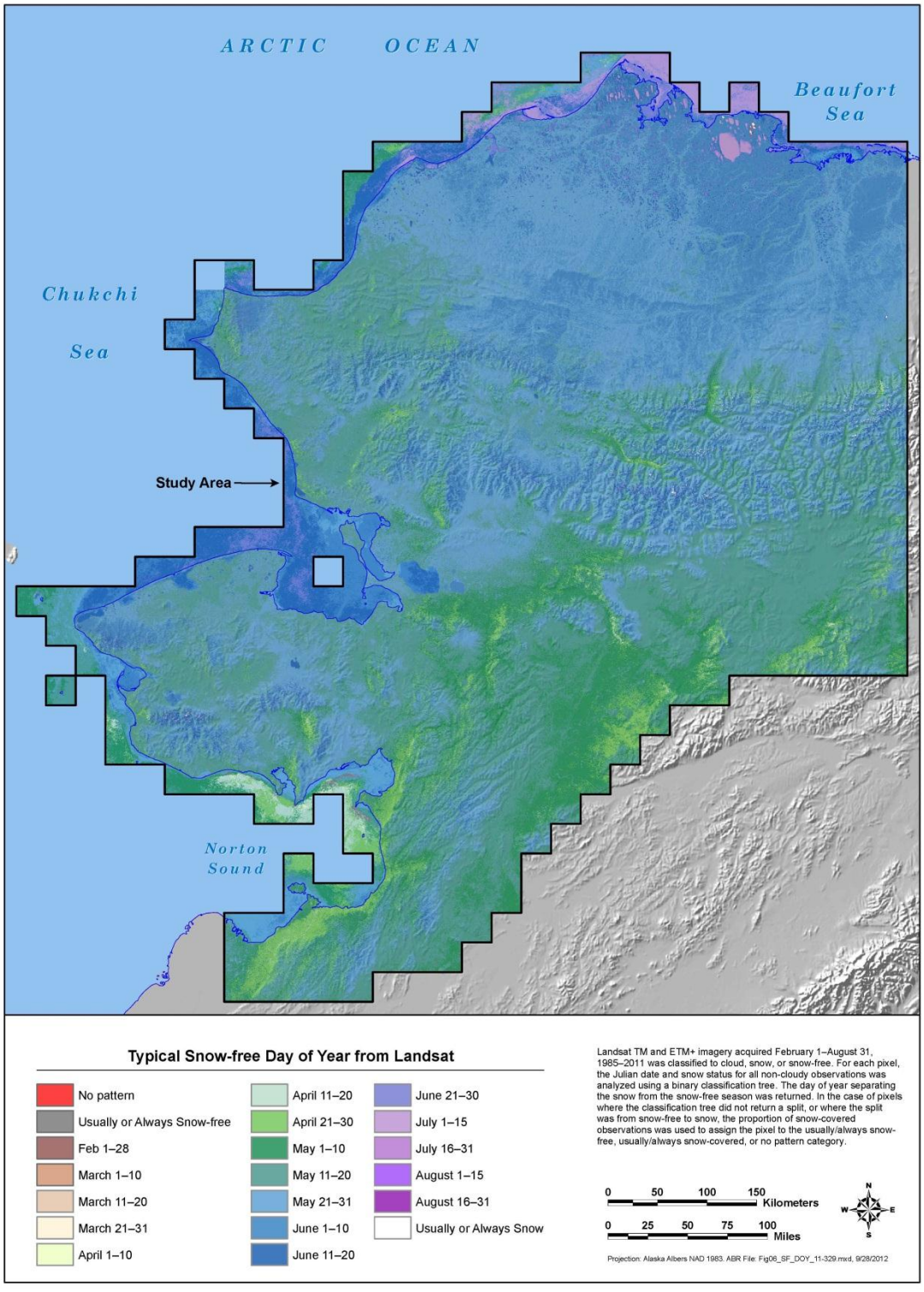

Figure 6. Typical snow-free day of year based on Landsat time series analysis, Western Arctic Caribou Herd Range, Alaska.

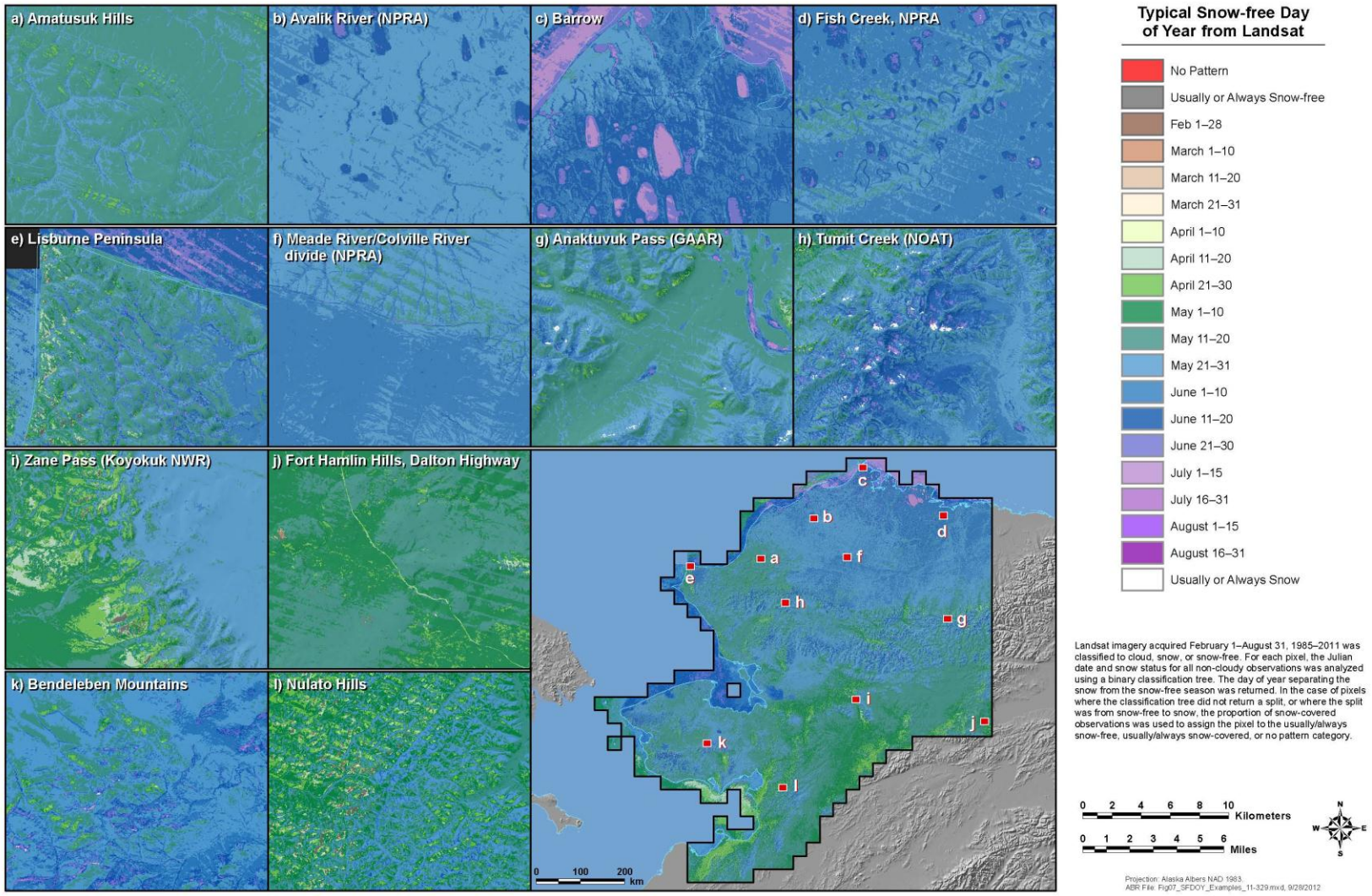

Figure 7. Examples of typical snow-free day of year based on Landsat time series analysis, Western Arctic Caribou Herd Range, Alaska.

dust on the snow surface) is observable in tile d (riparian dust) and j (road dust). Overall, the time series analysis appears to capture the sometimes drastic spatial variability of the landscape snow regime.

Striping artifacts are apparent throughout the map, for example tiles b/d/f. The stripes are the result of including Landsat 7 ETM+ SLC-OFF data with striped gaps in each scene. The results are different (generally by only a few days) when an influential scene near the snowmelt date has missing data in stripes. The maps (Figure 6 and 7) are symbolized with ten-day intervals (though the underlying data has one-day resolution); the appearance of stripes on the maps is somewhat arbitrary due to the particular cutpoints selected. The striping artifacts do limit the usefulness of the maps for characterizing snowmelt differences of up to 3-4 days—such small differences could easily be the result of the slightly different data inputs resulting from the SLC-OFF gaps.

The sample size for each pixel in the binary classification tree analysis was generally large (Figure 8), with an average value of 216 cloud-free observations and standard deviation of 33.6 observations. Pronounced wedge shapes in the sample size raster are caused by the overlap pattern of adjacent Landsat paths (Figure 3). There were more cloud-free observations in mountainous areas than in lowlands, suggesting that cloud cover is less frequent over mountains. Many of the highest sample sizes are in the east, where more Landsat images were collected (Figure 4). The lowest sample sizes occur offshore in the northern and western portions of the study area; Landsat satellites collected few scenes for path/rows that are mostly ocean, since the satellite is focused on land surface studies. Overall the high sample sizes provide adequate data for a robust analysis of snow persistence patterns on the landscape.

The no split condition occurred for 0.16% of the study area and was usually associated with situations where the pixel was nearly always snow-covered or nearly always snow-free. In these cases, the classification tree determined that the optimal split was no split, i.e., leaving all the data in one class. The proportion of observations with snow (p_snow) was used to categorize the "no split" cases. "Usually snow-free" ($p\_snow \leq 0.25$, pixel value 1) and "usually snow-covered" ($p\_snow \geq 0.25$, pixel value 254) each accounted for 0.08% of the study area. Most of the "usually snow-covered" pixels occurred in rugged mountainous terrain, mainly in the Brooks Range. Much of it appears to occur on permanent snowfields while some does become snow-free, at least during some summers. The shadowing in mountainous terrain is pronounced by late August; shadows are also darker in August than in midwinter because the surrounding terrain lacks bright snow which can reflect light into shadowed areas. The extreme shadowing could contribute to errors in the snow mapping for mid- to late-summer shadowed terrain because the signal to noise ratio in the satellite signal is particularly low. The only other location with sizeable patches of the "usually snow-covered" class occurred in some lakes east of Teshekpuk Lake; in this case the result appears to be spurious due to the highly variable sediment concentrations in the lakes, which confuses the snow mapping algorithm.

The "usually snow-free" class occurred occasionally in rugged mountainous terrain, rounded ridgetops, and barren floodplains—areas that are frequently windswept. Some extensive patches also occurred offshore in Norton Sound; these are probably spurious results. The "no pattern" class accounted for 0.01% of the study area. Much of this was offshore, again in Norton Sound, while other examples were scattered in small patches throughout the study area. Splits from

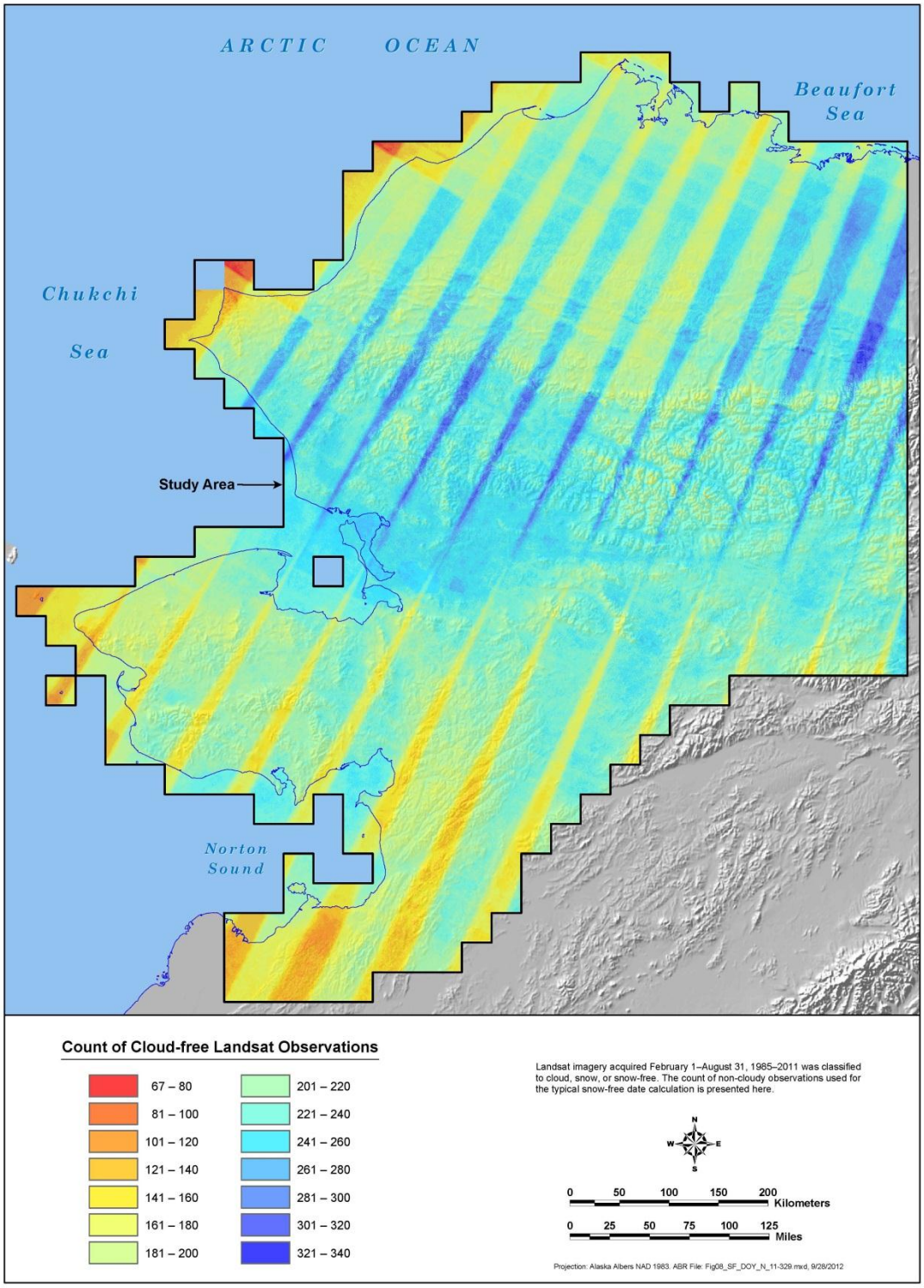

Figure 8. Count of cloud-free Landsat observations used to derive typical snow-free day of year based on Landsat time series analysis, Western Arctic Caribou Herd Range, Alaska.

snow-free to snow-covered were very rare (< than 0.0001% of the study area). They appeared to occur mostly in areas with deep terrain shadows.

Assessment and Validation

The internal consistency of the snow-free date model was estimated from the proportion of observations that were correctly classified by the snow-free date at each pixel (i.e. the sum of snow observations before snow-free date and snow-free observations on or after the snow-free date, divided by the total number of observations). The land portion of the study area, derived from the NLCD2001, is about 429,863 square kilometers (85% of the total study area). Some snow-covered sea ice and lake ice in the far north of the study area is included as "land" by this approach because it was not classified as "Open Water" in the NLCD2001. The snow mapping algorithm is expected to perform better over land, so the summary statistics focus on results for the land portion of the study area.

Incorrectly classified pixels can be caused by several different factors. Due to interrannual variation in the snowmelt date, some years will lack snow on dates prior to the snow-free date, and some will have snow on dates after the typical snow-free date. Similarly, though snow distribution patterns tend to repeat themselves across years, there are interannual variations in snow distribution patterns which will affect the distribution of snow cover during spring. Occasional summer snow events (especially at high elevations) can cause incorrectly classified observations. These are all examples of correct classification of the snow condition of pixels that do not conform to the typical pattern of snowmelt. Finally, snow mapping errors due to missed cloud cover, cloud shadows, or other factors contribute to incorrectly classified observations.

The internal consistency analysis indicated that 69.2% of the land in the study area had *p_correct* values of 95% or higher and an additional 29.5% had *p_correct* values between 90–95% (Table 5, Figure 9). These results demonstrate a strong internal consistency of the model results over land, where 98.8% of pixels had an internal correct classification rate of 90% or higher. Results were much less consistent for rivers, lakes and ocean; only 63.7% of the water in the study had an internal correct classification rate of 90% or higher.

Table 5. Summary of the percentage of observations correctly classified by the Landsat snow-free date algorithm.

Observations Correct (%)	Full Study Area (%)	Land Study Area (%)	Water Study Area (%)
< 75%	0.3%	0.0%	2.3%
75–90%	6.2%	1.2%	34.0%
90–95%	31.1%	29.5%	40.3%
95–97.5%	52.0%	57.4%	21.3%
97.5–100%	10.4%	11.9%	2.1%
	100.0%	100.0%	100.0%

Of the ten SNOTEL stations in the study area, nine collected suitable data (water equivalent and/or snow depth) during the snowmelt season for one or more years (Table 6). The number of years with data ranged from 1 year at Imnaviat Creek to 32 years at Bettles Field. Coldfoot had a

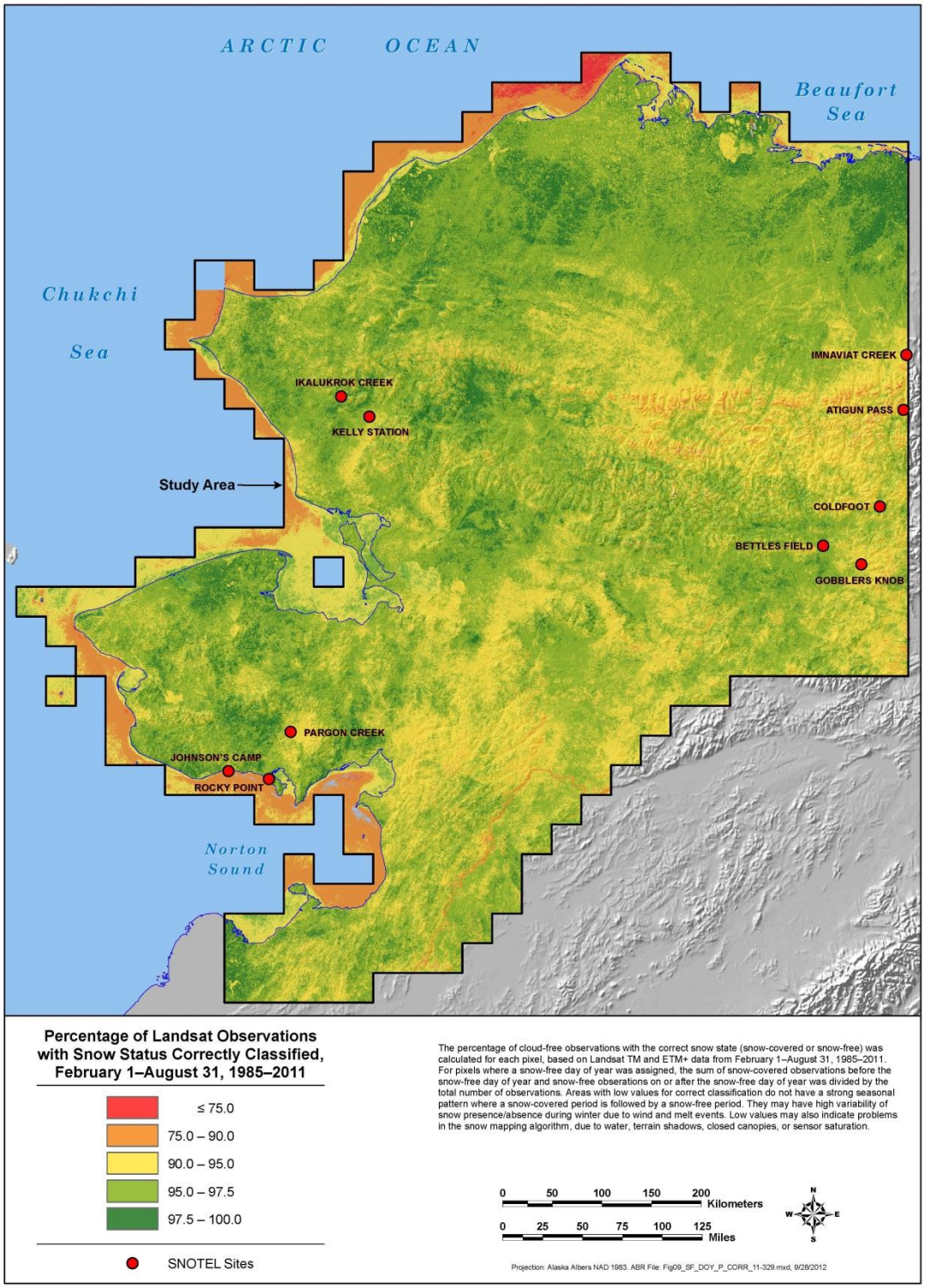

Figure 9. Proportion of cloud-free Landsat observations correctly classified by typical snow-free day algorithm, Western Arctic Caribou Herd Range, Alaska.

Table 6. SNOTEL data summary.

	Number of Years					Snowmelt Date			
SNOTEL Site	Snow Depth or SWE	Snow Depth	SWE	Earliest Year	Latest Year	SNOTEL (mean)	Landsat	SNOTEL (earliest)	SNOTEL (latest)
Atigun Pass	4	4	0	2009	2012	6 June	13 June	26 May 2011	12 June 2009
Bettles Field	32	1	32	1981	2012	16 May	14 May	28 April 2007	30 May 1985
Coldfoot	17	12	17	1996	2012	14 May	12 May	25 April 2007	25 May 2000
Gobblers Knob	6	6	0	2007	2012	n/a	8 May	10 February 2007	11 May 2008
Imnaviat Creek	1	1	0	2012	2012	2 June	27 May	2 June 2012	2 June 2012
Johnson's Camp	8	8	0	2003	2012	14 May	12 May	3 May 2003, 2009	29 May 2012
Kelly Station	4	1	4	1993	2012	17 May	18 May	7 May 2012	26 May 1994
Pargon Creek	7	7	0	2001	2010	12 May	16 May	14 April 2004	3 June 2001
Rocky Point	8	8	0	2002	2011	12 May	7 May	23 April 2004	27 May 2009

17 year record while the remaining six stations had record lengths of 4–8 years. Gobbler's Knob had six years of data but the data quality was problematic. There were extremely early melts in two of the years (February or March) but examination of the Landsat data from those years indicated that snow was present after the SNOTEL-derived snowmelt dates. There were also many gaps in the Gobbler's Knob data record, suggesting an unreliable snow depth sensor. For these reasons the Gobbler's Knob station data was excluded from the comparison.

The mean snowmelt dates from the eight remaining SNOTEL sites ranged from 13 May to 7 June although the dates were not evenly distributed. Six of the sites had SNOTEL snowmelt dates between 13 May and 17 May, while the other two (Atigun Pass and Imnaviat Creek) had SNOTEL snowmelt dates of 3 and 7 June, respectively. A comparison of the SNOTEL snowmelt dates and the Landsat time-series results (Figure 10) demonstrate very good agreement between the two estimates. The slope of the regression line was somewhat steeper than 1.0, suggesting a bias, though the influential late melting sites at Atigun Pass and Imnaviat Creek had few years of SNOTEL data (4 and 1 years, respectively). The correlation was high, with an r^2 value of 0.856.

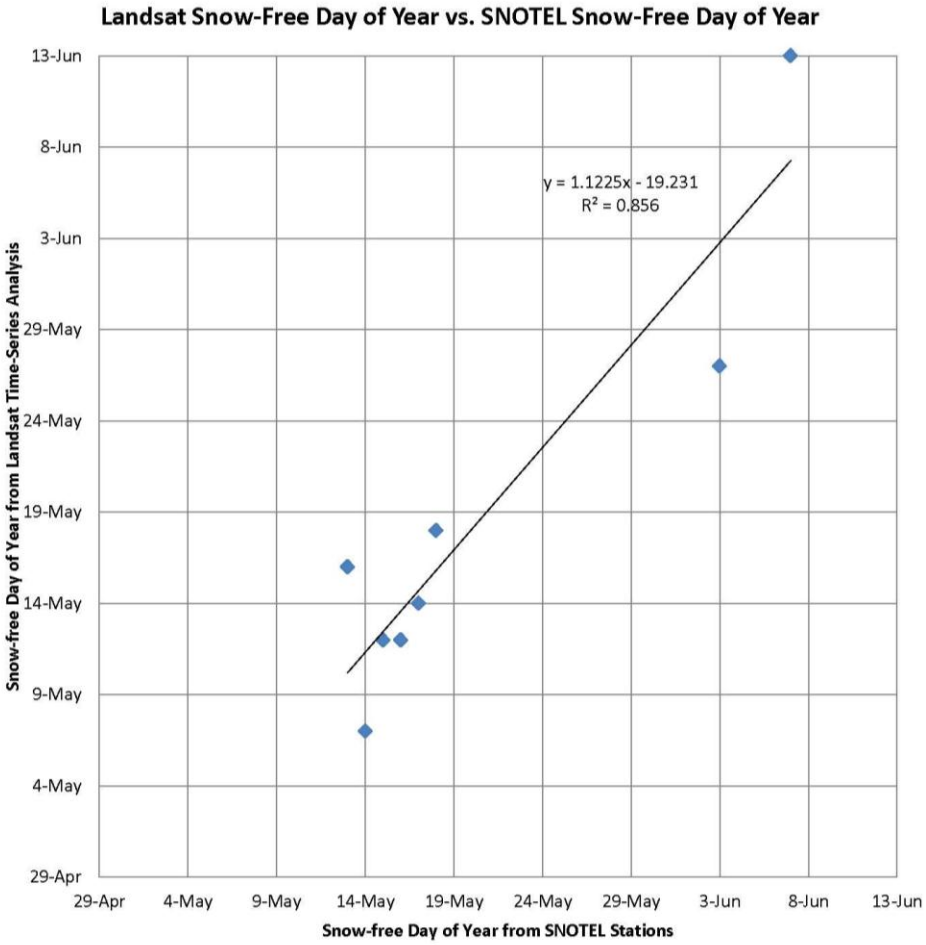

Figure 10. Comparison of Landsat-derived snow-free day of year and SNOTEL derived snow-free day of year, Western Arctic Caribou Herd Range, Alaska.

Discussion and Conclusions

The SNOTEL data are not necessarily more reliable than the Landsat-derived data for predicting the mean snowmelt date, particularly for stations with very short data records. The SNOTEL method required instrumentation maintained over many years to obtain data for eight points in the study area while the Landsat time series method used freely available archived imagery to estimate the snowmelt data for 562 million points in the study area. The good agreement between the two methods provides confidence in the spatially detailed results from the Landsat analysis.

Additional validation data could be obtained by compiling other records of annual snowmelt dates in the study area, such as field observations from the Imnaviat Creek site. If the study area were expanded to the west and south to include the Fairbanks area, then available SNOTEL records for snowmelt date become much more extensive for both number of sites and length of record.

Statewide snow metrics derived from MODIS imagery are currently being compiled by the Geographic Information Network of Alaska and the National Park Service. It would be useful to aggregate the Landsat results up to 500-m resolution and compare these to the average or median snowmelt date derived from the annual MODIS snow metrics. Finally, opportunistically collected oblique landscape images, especially those acquired during the active snowmelt period, could be compared to simulated views generated by the Landsat snowmelt date algorithm draped over the terrain. For oblique photos to be most useful it is important to have an accurate location (preferably including elevation and orientation). It would also be useful to include as much land surface within the frame as possible and to minimize sky coverage, though the horizon line is important.

Early and late melting terrain is readily identified for localized areas by the results of the snowmelt date analysis. For a given area, earlier melting areas have shallower snow than areas that melt later. However, simple date thresholds are unlikely to work to identify areas of shallow or deep snow across the study area because the snowmelt date is affected by other factors in additional to snow depth (mainly temperature) that vary with elevation, latitude, and region. Focal analysis to determine the difference between the snowmelt date for a pixel, and the mean snowmelt date for a surrounding window could provide a systematic measure of “early”, “normal”, and “late” that corresponds to “shallow”, “moderate”, and “deep” snow. Stratification based on elevation should be applied because colder temperatures at higher elevations delay snowmelt. Other stratification categories could include aspect and vegetation class. To facilitate stratification by vegetation class, this product is coregistered with another Landsat-derived product, the NLCD2001 land cover product.

For local study areas with highly variable snow cover, the Landsat-derived snowmelt date can be correlated with detailed field survey observations to improve snow distribution models. Much of the local variation in snow depth and snow water equivalent can be explained by snow persistence patterns captured by the Landsat analysis (e.g. Attachment 1 in Macander et al. 2012).

Changes in the average snowmelt date over time are a potential source of error for the current analysis. Although the input data are nominally from the 1985–2011 time period, the great

majority of the input data is from 2000 or later (Table 3); this shorter time frame should minimize the impact of changes in the snow regime. The inclusion of the 1985–1999 data increases the sample size of data available for the analysis, improving the ability to capture patterns of snow persistence on the landscape. In addition, all of the earlier data is gap-free since it is unaffected by the May 2003 scan-line corrector malfunction on Landsat 7. The additional gap-free data likely reduces the occurrence of striping artifacts.

The Landsat archive compiled for the snow persistence analysis could have many other useful applications unrelated to snow. Although the snow persistence algorithm used only data from the February 1–August 31 date range, the entire Landsat Thematic Mapper (TM) and Enhanced Thematic Mapper+ (ETM+) archive was reviewed and all available scenes with some useful (i.e. cloud-free) portions were compiled. All of the useful TM and ETM+ scenes acquired from September 1984–September 2011 are included with the data deliverables. These data could be used to perform spectral change detection using scenes from the mid-summer, peak phenology time period. A similar change detection analysis focused on coastal changes (e.g. coastal erosion) could utilize late summer and early fall imagery, when the sea ice is generally absent and cloud cover is lower. Atmospheric correction and refinement of cloud masking would improve the sensitivity of spectral change detection efforts, though it would be not be as necessary for assessments based on human interpretation.

Literature Cited

Chander, G., B. L. Markham and D. L. Helder. 2009. Summary of current radiometric calibration coefficients for Landsat MSS, TM, ETM+, and EO-1 ALI sensors. Remote Sensing of Environment 113:893–903.

Hall, D. K., G. A. Riggs, and V. V. Salomonson. 1995. Development of methods for mapping global snow cover using Moderate Resolution Imaging Spectroradiometer data. Remote Sensing of the Environment 54:127–140.

Hall, D.K., G.A. Riggs, and V.V. Salomonson. 2001. Algorithm Theoretical Basis Document (ATBD) for the MODIS Snow and Sea Ice-mapping Algorithms, September 2001. MODIS Snow and Sea Ice Global Mapping Project, Goddard Space Flight Center, Greenbelt, MD. http://modis-snow-ice.gsfc.nasa.gov/atbd.html (accessed 20 January 2006).

Irish, R. R., J. L. Barker, S. N. Goward, and T. Arvidson. 2006. Characterization of the Landsat 7 ETM+ Automated Cloud-Cover Assessment (ACCA) Algorithm. Photogrammetric Engineering & Remote Sensing 72(10):1179–1188.

Macander, M. J., E. R. Pullman, C. S. Swingley, K. L. Beattie, and W. A. Davis. 2012. Snow distribution surveys, mine study area. Appendix 7.2D to Chapter 7.2, Surface Water Hydrology—Bristol Bay Drainages. Pebble Environmental Baseline Document. Prepared for Pebble Limited Partnership by ABR, Inc.

Masek, J. G., E. F. Vermote, N. E. Saleous, R. Wolfe, F. G. Hall, F. Huemmrich, F. Gao, J. Kutler, and T. K. Lim. 2006. A Landsat surface reflectance data set for North America, 1990-2000. IEEE Geoscience and Remote Sensing Letters 3(1):69–72.

M. J. Brodzik, R. L. Armstrong, and M. Savoie. 2007. Global EASE-Grid 8-day Blended SSM/I and MODIS Snow Cover. National Snow and Ice Data Center, Boulder, Colorado.

Roy, D.P., J. Ju, K. Kline, P. L. Scaramuzza, V. Kovalskyy, M. C. Hansen, T. R. Loveland, E. F. Vermote, and C. Zhang. 2010. Web-enabled Landsat Data (WELD): Landsat ETM+ composited mosaics of the conterminous United States. Remote Sensing of Environment 114:35-49.

Sturm, M., J. Holmgren, and G. E. Liston. 1995. A seasonal snow cover classification for cocal to global applications. Journal of Climate 8:1261–1283.

Sturm, M., J. P. McFadden, G. E. Liston, F. S. Chapin III, C. H. Racine, and J. Holmgren. 2001. Snow-shrub interactions in Arctic tundra: a hypothesis with climatic implications. Journal of Climate 14:336–344.

Appendix A: Data Deliverable

The data deliverable includes the results of the time series analysis and several diagnostic rasters. The deliverable also includes the extensive Landsat archive compiled for the analysis, in several different formats.

Results: The results of the analysis including sf_doy, n, and p_correct.

Ancillary: Landsat WRS2 path/rows, Alaska 30km tiles, Overlap pattern, and the WACH range polygons.

Browse: This directory is organized by WRS2 path/row and it includes all of the browse images (in .jpg format) for all the TM and ETM+ scenes in the USGS archive that cover the study area, including scenes that were not acquired for the current analysis (mostly because they had extensive cloud cover). There is a text file (.meta) for each browse image that was also obtained from USGS. These are the same browse images that are available via the Glovis viewer, though they are faster to display when stored locally. Two refinements were made to the standard browse product. First, an ArcGIS compatible world file was created based on the parameters in the .meta file. Second, the browse file was renamed, prepending the date (in mm_dd_yyyy format) to each file. This allows the scenes to be sorted in day of year order, regardless of sensor or year.

Raw: The L1G and L1T files downloaded from USGS for each scene. All of the files from the USGS download are included; however, the .tar.gz file has been unpacked. To save disk space each individual TIFF file has been compressed using gzip compression.

Fullres: Full resolution seven-band images for each TM and ETM+ scene were calibrated to top of atmosphere reflectance (and temperature brightness, for the thermal band). Each scene was then converted to an 8-bit format following MRLC conventions. The resulting image was encoded in lossless JP2 format and auxiliary files were created to facilitate viewing of the images using the “standard deviation” or “minimum/maximum” stretch in ArcMap. Suggested band combinations are natural color (3/2/1), color infrared (4/3/2), and false color infrared (5/4/3 or 7/4/3).

Tiles: The tile folders contain the tiled data for all of the Landsat scenes that overlap a particular tile. The cloud mask (lndcsm) and cloud/shadow/snow map (css) products are included in addition to the raw imagery, calibrated to top-of-atmosphere reflectance (lndcal). The imagery is organized first by column (Hxxx) then by row (Vxx) then by parameter (lndcal, lndcsm, css).

The Department of the Interior protects and manages the nation's natural resources and cultural heritage; provides scientific and other information about those resources; and honors its special responsibilities to American Indians, Alaska Natives, and affiliated Island Communities.

NPS 953/117759, December 2012

National Park Service
U.S. Department of the Interior

Natural Resource Stewardship and Science
1201 Oakridge Drive, Suite 150
Fort Collins, CO 80525

www.nature.nps.gov